RSC Advances

ROYAL SOCIETY OF CHEMISTRY

www.rsc.org/advances

Journal Name

ARTICLE

Controllable synthesis of core-satellites Fe_3O_4@Polypyrrole/Pd nanoarchitectures with aggregation-free Pd nanocrystals confined into Polypyrrole satellite as magnetically recoverable and highly efficient heterogeneous catalysts

Received 00th January 20xx,
Accepted 00th January 20xx

DOI: 10.1039/x0xx00000x

www.rsc.org/

Wanchun Guo*[a], Jiao Jiao[a], Kesong Tian[a], Yongfu Tang[a], Yin jia[a], Ruifei Li[a], Zhaopeng Xu[b], Haiyan Wang[a]

A soft template-assisted simultaneous redox strategy has been developed to fabricate Fe_3O_4@Polypyrrole/Pd (Fe_3O_4@PPy/Pd) nanocomposites with single Fe_3O_4 core and multiple PPy satellites, into each of which multiple tiny Pd nanocrystals are uniformly confined. The dispersion of Pd nanocrystals into PPy satellite and the Pd loading of the nanocatalyst could be finely tuned by tailoring the polarity of the reaction medium and by changing the molar ratio of pyrrole monomer to Pd precursor, respectively. The Pd-based catalyst shows high activity, robust stability and magnetic recyclability for the reduction of nitroaromatic compounds. Superior activity could be attributed to the short transport route toward the active Pd nanocystals within the small PPy satellite for the outer substitutes. Meanwhile, high stability could be ascribed to the confinement of Pd nanocrystals uniformly into PPy satellite against aggregation and even loss of active sites during catalytic transformations.

Introduction

Magnetic nanocomposite-supported noble-metal nanoparticles as one of the most important heterogeneous nanocatalysts are currently of increasing interest for liquid-phase catalysis in carbon-carbon coupling reactions, hydrogenation, olefin oxidations, and so on, because of their facile recoverability after the reactions only by using an external magnetic field.[1-5] In particular, extensive efforts have been devoted to anchor noble-metal nanoparticles onto magnetic nanoarchitectures with both magnetic nanoparticles as inner cores and inorganic materials or organic polymers as outer shells, such as Fe-Ni@C,[6] Co@C,[7] Fe_3O_4@C,[8, 9] Fe_2O_3@SiO_2,[10] Fe@SiO_2,[11] Fe_3O_4@SiO_2,[12-13] Fe_3O_4@PPy,[14] Fe_3O_4@PANI,[15] and Fe_3O_4@PEGDMA.[16] These nanoscale coatings not only protect magnetic nanoparticles from corrosion during catalytic reactions but also make small noble-metal nanoparticles highly dispersed on their surface, thereby exposing numerous catalytically active sites and giving a great accessibility to the reactants to retain the initial high activity of noble-metal nanoparticles. Unfortunately, metal particles located onto magnetic supports commonly suffer from undesirable aggregation or shape-change in catalytic transformations, thereby resulting in a dramatic decrease in their initial activity, possibly owing to their high surface energy and much weak interaction between metal nanoparticles and magnetic scaffolds.

Confining noble-metal nanoparticles within magnetic supports has been proved to be one of the most promising concepts to design highly stable magnetic nanocatalysts. Yin et al.[17] and Zhao et al.[18, 19] reported different multistep synthesis strategies to encapsulate Fe_3O_4@SiO_2 and Fe_3O_4@C supported noble-metal nanoparticles into an extra-porous SiO_2 coating, respectively. On the basis of synthesis strategies mentioned above, Cui et al.[20] prepared yolk-shell Fe_xO_y/Pd@mesoporous-SiO_2 nanoreactors as a heterogeneous catalyst by sacrificing the middle carbon shell. Zhang et al.[21] synthesized double-shell Fe_3O_4@TiO_2/Au@Pd@TiO_2 nanostructures through multilayer coating strategy and subsequent selective removal of SiO_2 middle layer. Hur et al.[22] Prepared dual Pd and $CuFe_2O_4$ nanoparticles embeded into silica microspheres. Recently, Chen et al.[23] and Zhu et al.[24] fabricated different M-Fe_3O_4@MOF (M=Au, Pt, Pd) core-shell nanocatalysts by entrapping noble-metal particles on inner Fe_3O_4 cores into outer metal-organic framework, respectively. Cui et al.[25] and Zhang et al.[26] designed Au

[a] Key Laboratory of Applied Chemistry of Hebei Province
College of Environmental and Chemical Engineering
Yanshan University
Qinhuangdao 066004 (P. R. China)
Tel./Fax: (+86)-335-8061-569
E-mail:gwc333744@126.com.
[b] Key Laboratory for Special Fiber and Fiber Sensor of Hebei Province
College of Environmental and Chemical Engineering
Yanshan University
Qinhuangdao 066004 (P. R. China).

Electronic Supplementary Information (ESI) available: FT-IR, XRD and TG curves of samples, catalytic data of other nitroaromatic compounds. See DOI: 10.1039/x0xx00000x

and Pd nanoparticles enveloped into polypyrrole/Fe_3O_4 composite hollow capsules, respectively. Our previous works[27, 28] reported in situ confined growth of Au nanoparticles into pH responsive magnetic cross-linked Poly(4-vinylpyridine) frameworks to inhabit aggregation and loss of catalytic active species, thus enhancing their stability. The framework of magnetic scaffolds outside metal active sites provides a strong spatial hindrance to enhance the stability against their agglomeration and loss during catalytic transformations. In the meantime, the pores of the outer shell around metal nanoparticles enable an accessibility of outer chemical species towards entrapped active sites. However, embedding noble-metal nanoparticles deeply into the matrix of magnetic supports may suppress mass transfer of the reactant species and ultimately result in a decrease in their catalytic activity and utility. Meanwhile, fabrication of the metal nanoparticles and outer solid frameworks in individual steps also makes the whole synthetic procedure of magnetic catalysts quite complicated, which limits practical applications of this kind of catalysts. Accordingly, it is highly desired but still is a troublesome issue to fabricate highly efficient magnetic nanocatalysts with aggregation-free noble-metal nanoparticles by means of a facile strategy.

PPy@Pd nanocomposites, such as nanocapsules,[29] and nanotubes,[30, 31] TiO_2@PPy@Pd nanofibers,[32] and Graphene nanosheets-polypyrrole/Pd[33] have been drawn great attention, due to strong chemical affinity of pyrrole groups for Pd nanoparticles and good electronic conductivity of PPy. Especially, one-pot synthesis of Ppy@Pd composite catalysts, such as Ppy@Pd nanospheres,[34, 35] PS@Ppy/Pd nanocomposites,[36, 37] Fe/C-PPy-Pd nanocomposites microspheres,[38] and reduced graphene oxide (rGO)/Pd-Fe_3O_4@polypyrrole (PPy),[39] via simultaneous redox reaction between pyrrole monomers and Pd(II) precusors provides an ingenious idea to design catalysts for us. Herein, we report a facile soft template-assisted strategy to synthesize core-satellites Fe_3O_4@PPy/Pd nanostructures with single Fe_3O_4 nanocluster as inner core and Ppy particles encapsulating multiple highly dispersed Pd nanocrystals as outer satellites on the basis of direct redox reaction between pyrrole monomers and H_2PdCl_4. With Polyvinylpyrrolidone macromolecules in the form of irregular random coils modified on Fe_3O_4 nanocluster as soft-templates, the redox potential difference between pyrrole and H_2PdCl_4 drives in situ generation of multiple PPy/Pd satellites, with multiple fine Pd nanocrystals confined uniformly into a single small PPy satellite, onto a single Fe_3O_4 core. Confinement of the highly dispersed Pd nanocrystals within PPy satellites not only improves stability of Pd nanoparticles to avoid aggregation and loss, but also promotes their reactivity and utility. It is attributed to that outside chemical species around these satellites could take relatively short diffusion route towards active sites distributed uniformly into small PPy satellites. As expected, the as-synthesized Pd-based magnetic nanocatalysts exhibit outstanding activity, facile magnetic recoverability, and stable recyclability towards the reduction of nitroaromatic compounds such as 4-Nitroaniline (4-NA), 3-Nitroamine (3-NA), 2-Nitroaniline (2-NA), 2-Nitrophenol (2-NP), 3-Nitropheol (3-NP), 4-Nitrophenol (4-NP), 1-Chloro-2-nitrobenzene, and 2-Amino-5-nitrophenol.

Experimental

Materials

Ferric chloride hexahydrate ($FeCl_3 \cdot 6H_2O$, 98%), 3-Nitrophenol (3-NP), 3-Nitroaniline (3-NA), 1-Chloro-2-nitrobenzene, and 2-Amino-5-nitrophenol were acquired from Alfa Aesar. Poly (acrylic acid) (PAA; Mw=1,800) was obtained from Sigma–Aldrich. Sodium acetate (NaAc) and ethylene glycol (EG) was gained from Guangzhou Guanghua Chemical Reagent Co., Ltd. Polyvinylpyrrolidone (PVP; Mw=58,000), 2-Nitroaniline (2-NA), 4-Nitroaniline (4-NA), 2-Nitrophenol (2-NP), 4-Nitrophenol (4-NP), were obtained from Aladdin. $PdCl_2$ (99%) was obtained from CIVI-CHEM. Ethanol and Sodium borohydride ($NaBH_4$) were got from Tianjin Guangfu Fine Chemical Research Institute. Pyrrole (≥98%, Sinopharm Chemical Reagent Co., Ltd.) was used after distillation under reduced pressure. Deionized water was prepared and used through the experiments.

Preparation of Fe_3O_4@PPy/Pd nanocomposite with core-satellites structure

The PAA-modified Fe_3O_4 nanoclusters were synthesized through a solvothermal method according to our previous literature.[27] To prepare Fe_3O_4@PPy/Pd nanocomposite, PAA-modified Fe_3O_4 nanoparticles (0.1 g) were firstly dispersed into an aqueous solution of PVP (20 mL, 25 g/L) by means of ultrasonication, and then were vigorously shaken for 24 h at 25 ^oC to make sure that the surface of Fe_3O_4 was modified by PVP. Then the obtained products were rinsed with distilled water three times to remove redundant PVP.

Subsequently, the above obtained PVP-modified Fe_3O_4 nanoparticles were re-dispersed in mixed solvent (150 mL) of distilled water and absolute ethanol in different volume ratio under ultrasonication, followed by the addition of pyrrole monomer (0.1 mL, 1.4 mmol). After being transferred into a three-necked flask (250-mL capacity), the homogenous suspension was incubated and stirred at 2 ^oC for 12 h to allow absorption of pyrrole onto the PVP-modified Fe_3O_4, followed by the addition of a certain amount of H_2PdCl_4 solution (56 mM) to induce reaction. The redox reaction was conducted under strong mechanical stirring at 2 ^oC for 12 h. These as-synthesized products were separated magnetically, rinsed with ethanol and water several times, and then dried at 60 ^oC for 12 h.

Catalytic performance of Fe_3O_4@PPy/Pd nanocomposites for reduction of the nitroaromatic compounds

The catalytic performance of Fe_3O_4@PPy/Pd was evaluated by the reduction of the nitroaromatic compounds including 4-NP, 3-NP, 2-NP, 4-NA, 3-NA, 2-NA, 1-Chloro-2-nitrobenzene, and 2-Amino-5-nitrophenol by $NaBH_4$. Catalytic reduction of 2-NA is just an example. Typically, an aqueous solution of 2-NA (2 mL, 5 mM) was mixed with the above obtained catalyst suspension (0.1 mL, $4.42*10^{-6}$ mmol of Pd, 0.0442 mol%), followed by the addition of fresh aqueous $NaBH_4$ solution (20 mL, 0.2 M). The filtered solution samples were monitored by UV/Vis spectroscopy every 3 minute until the mixture became colorless.

The recyclability of the magnetic catalyst was also studied by the reduction of 2-NA under the same reaction parameters. The nanocatalyst recovered magnetically was washed and subsequently applied to the next cycle.

Characterization

TEM and SEM images were acquired using a HT 7700 electron microscope (HITACHI) and a SUPRA 55 schottky field emission scanning electron microscope, respectively. HRTEM images were gained with a JEM-2010 electron microscope operated at 200 kV. FT-IR spectra of samples were recorded utilizing a Nicolet IS10 infrared spectrometer with KBr pellets. X-ray diffraction (XRD) patterns of the products were recorded on a RIGAKU SmartLab X-ray diffractometer with Cukα radiation (λ=0.15418 nm) at 40 kV. Shimadzu UV 2550 spectrophotometer was utilized to monitor the spectral absorption of nitroaromatic compounds at different intervals during the catalytic reaction. The X-ray photoelectron spectroscopy (XPS) analysis was used to ananylze chemical state of Pd element by using an ESCALAB 250 Xi spectrometer with an $Al_{K\alpha}$ X-ray source. Thermogravimetric analysis (TGA) was acquired with a NETZSCH STA-449 C instrument in nitrogen flow at a heating rate of 10 K/min ranging from room temperature to 900 ^{o}C. Magnetic data of samples was got with a Lake Shore-7407 vibrating sample magnetometer. The contents of Pd species in different Fe_3O_4@PPy/Pd nanocomposites were measured using AGILENT-725 inductively coupled plasma atomic emission spectrometer (ICP-AES).

Results and Discussion

Fe_3O_4@PPy/Pd nanocomposites with core-satellites structure were rationally designed and successfully synthesized on the basis of simultaneous redox reduction of pyrrole monomer and H_2PdCl_4 on the surface of Fe_3O_4 nancoclusters with PVP random coils as soft-templates, as depicted in scheme 1. In this study, PAA-modified Fe_3O_4 nanoclusters were firstly fabricated by a simple hydrothermal method.[27] The carboxyl groups tethered onto Fe_3O_4 nanoclusters enable high dispersion of them into polar solvents such as water and absolute ethanol. Normally, amphiphilic PVP macromolecules in good solvents such as water and ethanol have a steric configuration of loose random coils due to the non-cross linked long chains with high weight-average molecular weight up to 58,000.[40, 41] Accordingly, following the modification onto Fe_3O_4 nanocluters with the assistance of the hydrogen-bond interaction between pyrrolidone groups in PVP and carboxyl groups in PAA,[42] PVP molecules preserve their configuration of irregular random coils. When pyrrole, hydrophobic monomer, was added into the dispersion of PVP-modified Fe_3O_4 nanoclusters in mixed solvents, numerous pyrrole species diffuse homogenously into irregular PVP random coils driven by the strong affinity of the highly polar pyrrolidone moieties to pyrrole monomers as proton donors.[43] Subsequently, pyrrole monomers dispersed into PVP coils can be in situ oxidized to PPy by the addition of H_2PdCl_4, and simultaneously H_2PdCl_4 itself can be in situ reduced to Pd nanoparticles, on the basis of the polymerization of pyrrole oxidized by Pd precursor.[36, 37] Finally, with multiple irregular PVP random coils onto a single Fe_3O_4 nanocluster as soft templates, Fe_3O_4@PPy/Pd nanocompsites, with single Fe_3O_4 nanocluster as core and multiple PPy/Pd hybrid particles as satellites, are successfully synthesized by finely tailoring the redox rate between H_2PdCl_4 and pyrrole monomers. Multiple fine Pd nanoparticles are uniformly confined into a small PPy satellite in PPy/Pd nanocomposites, which enhances the stability of Pd species against agglomeration and loss during catalytic transformations, and greatly facilitates mass transfer of the reactants outside PPy satellites towards the active sites by taking the short diffusion route through small PPy satellites, thus promoting catalytic activity of Fe_3O_4@PPy/Pd nanocompsites.

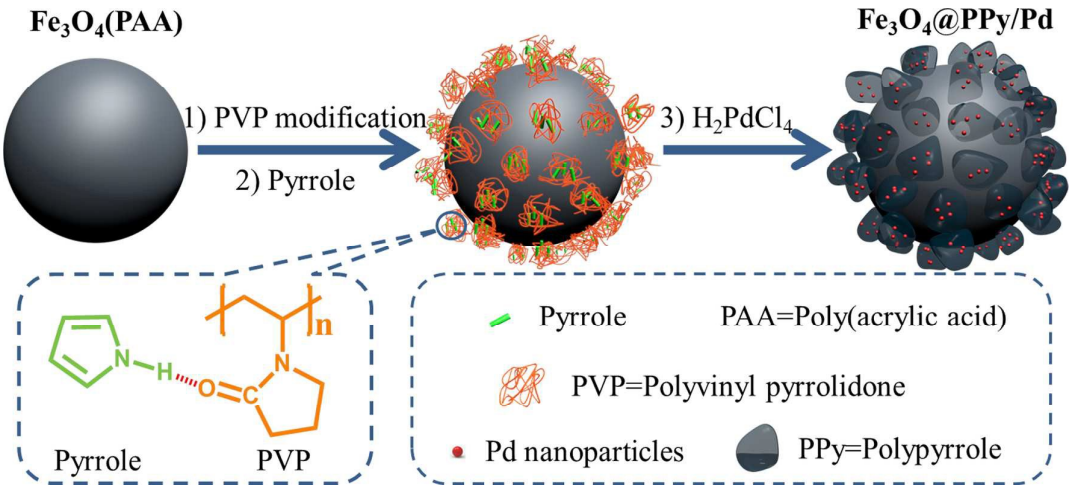

Scheme 1 Synthetic illustration of Fe_3O_4@PPy/Pd nanocomposites

Preparation of Fe_3O_4@PPy/Pd nanocomposites with a core-satellites structure

The PAA-modified Fe_3O_4 nanoclusters were fabricated through a facile solvothermal route in accordance with our previous report.[27] Fig. 1a, d displays the TEM and SEM images of the PAA-modified Fe_3O_4 nanoclusters. The monodispered Fe_3O_4 nanoclusters with the average particle size of approximately 200 nm have a uniform spherical shape. Abundant carboxyl functional groups onto Fe_3O_4

nanoclusters endow them with good dispersion in polar solvents such as water or ethanol, which is extremely beneficial to generate well-defined core-shell magnetic nanospheres such as Fe_3O_4@SiO_2[17] and Fe_3O_4@resorcinol-formaldehyde resin.[44] Subsequently, PVP molecules with high molecular weight were absorbed onto PAA-modified Fe_3O_4 nanoclusters based on the hydrogen-bond interaction between pyrrolidone groups in PVP and carboxyl groups in PAA. After adding pyrrole and H_2PdCl_4 successively into the dispersion of PVP-remodifed Fe_3O_4 nanoclusters in mixed solvent of water and ethanol at 2 ^oC, the color of the above dispersion changed from brown to quite black with the prolonging time, involving the simultaneous generation of Pd nanoparticles and PPy due to the redox reaction between pyrrole and H_2PdCl_4. As shown in Fig. 1b, as-prepared Fe_3O_4@PPy/Pd nanocomposites are composed of single Fe_3O_4 core and multiple irregular PPy/Pd satellites in good agreement with the SEM image (Fig. 1f), in which the resultant nanocomposites are relatively uniform in size and raspberry-like in shape. Irregular structure of PPy satellites is probably consistent with that of PVP soft templates onto inner Fe_3O_4 core, because the amphiphilic property of PVP molecules with high molecular weight of approximately 58,000 enables the presence of molecules in the form of irregular random coils at nanoscale in good solvents such as water and ethanol.[40, 41] From the HRTEM image with higher resolutions (Fig. 1c, d), it is evident that the size of irregular PPy/Pd satellites ranges from 20 to 30 nm and multiple monodispersed Pd nanoparticles with an uniform particle size of approximately 4-5 nm are uniformly confined into single PPy satellite. The HRTEM image in Fig. 1d shows the inter-planar spacing of small crystal particles is 0.234 nm, which could be assigned to the Pd^0 (111) plane.[45] In addition, it is obviously observed that the homogeneous Pd nanoparticles in a finely divided state are confined spatially into single PPy particle without any agglomeration of metal nanoparticles, indicating that this simultaneous redox strategy with PVP random coils as soft templates is highly efficient for in situ confined growth of agglomeration-free Pd nanoparticles. When using the above magnetic nanocomposites for heterogeneous catalysis in liquid phase, PPy frameworks would protect Pd nanocrystals uniformly distributed into them against migration and even agglomeration, resulting in promoted stability. Moreover, chemical species around small PPy satellites could take shorter transport route across them towards metal active sites embedded into them than those embedded deeply into solid supports, thereby enhancing catalytic activity and utility of Pd nanocystals. As depicted in EDS mapping images (Fig. 1g, h), the homogeneous distribution of Pd element into the samples further confirms that Pd nanoparticles are highly dispersed into the PPy structure.

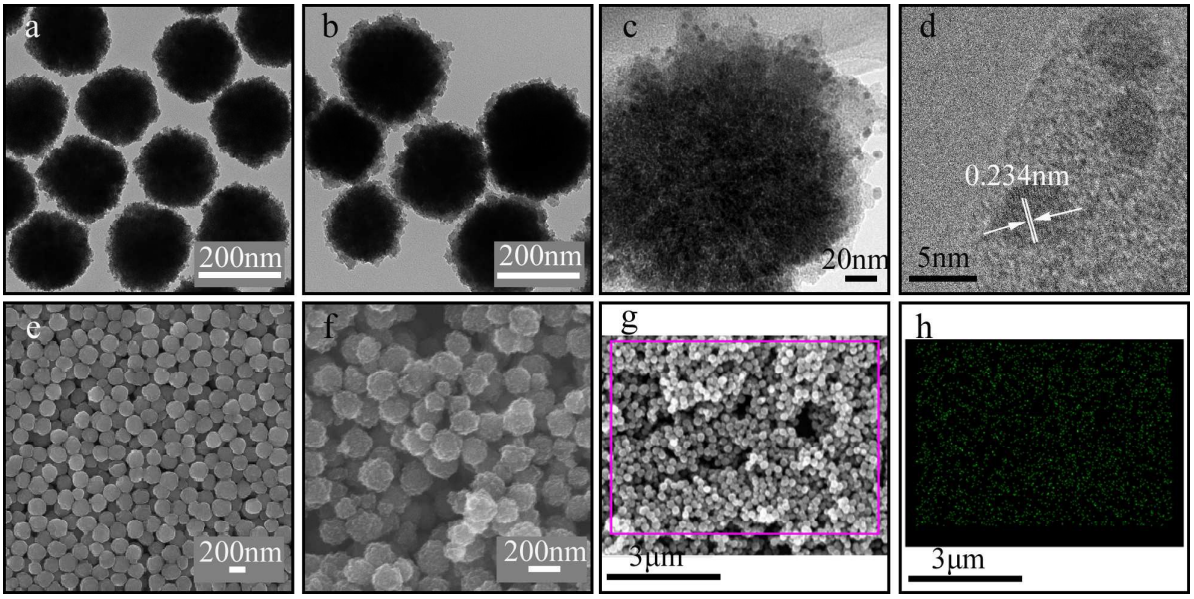

Fig. 1 TEM (a) and SEM (e) images of PAA-modified Fe_3O_4, TEM (b) and SEM (f) images of the resultant Fe_3O_4@PPy/Pd nanocomposites, HRTEM images (c, d), SEM image (g) and Pd elemental map (h) of Fe_3O_4@PPy/Pd nanocomposites

FT-IR spectroscopy was also used to investigate chemical structure of Fe_3O_4@PPy/Pd nanocomposites (Fig. S1). The peak at 583 cm^{-1} is ascribed to the Fe-O vibrations,[46] consistent with that of PAA-modified Fe_3O_4 nanoclusters in Fig. S1a. The broad absorption at 3423 cm^{-1} could be attributed to stretching vibration of N-H bonds in PPy and O-H bonds in PAA. The peaks at 1559 cm^{-1} and 1453 cm^{-1} correspond to stretching vibrations of C=C and C-N bonds in the pyrrole ring, respectively.[47] Furthermore, the peaks at 1332 cm^{-1}, 1049 cm^{-1} and 934 cm^{-1} could be attributed to C-N in-plane,[48] N-H in-plane[49] and C=C out-of-plane deformation vibrations[47] in the pyrrole ring, respectively. The weak absorption band at 1208 cm^{-1} is responsible for C-C breathing vibration in the pyrrole ring.[50] All these results mentioned above could confirm the formation of PPy onto Fe_3O_4 nanoclusters. Fig. S3 shows the thermogravimetric analysis (TGA) of PAA-modified Fe_3O_4 nanoclusters and Fe_3O_4@PPy/Pd nanocomposites. The weight losses of two above samples ranging from room temperature to 800 ^oC are about 15 and 36 wt%, respectively, and the difference of the weight loss (21 wt%) could result mainly from the degradation of PPy, which further suggests the successful construction of PPy onto Fe_3O_4

nanoclustes.To gain further insights to the structure of Fe_3O_4@PPy/Pd nanocomposites, XRD analysis of the samples (Fig. S2) was performed. XRD pattern of Fe_3O_4 nanoclusters in Fig. S2a exhibits six diffraction peaks, which at 2θ = 30.1, 35.6, 43.1, 53.6, 57.1, and 62.7° correspond to (220), (311), (400), (422), (511), and (400) characteristic peaks of face-centered cubic Fe_3O_4 phase (JCPDS card No. 19-0629), respectively. As shown in Fig. S2b , besides those six peaks of cubic Fe_3O_4 phase, no any other obvious signal was observed in the XRD pattern of Fe_3O_4@PPy/Pd nanocomposites synthesized in mixed solvent with the ethanol/water volume ratio at 1:1. It is probably attributing to homogeneous dispersion of tiny Pd nanocrystals into Ppy matrix,[45] in good agreement with the TEM result of magnetic nanocomposites in Fig. 1c. To clarify further existence of Pd nanocrystals in magnetic nanocomposites, XRD was also utilized to measure the fine structure of Fe_3O_4@PPy/Pd nanocomposites synthesized in pure water. As revealed in Fig. S2c , three newly emerging peaks at 2θ = about 39.9, 46.2, and 67.5° could be assigned to the characteristic peaks of Pd nanocystals related to (111), (200), and (220) plane(JCPDS No. 65-2876), respectively, being attributed to the formation of numerous aggregates of Pd nanocrystals in this nanostructure (Fig. 2a), which provides some indirect evidence for the generation of Pd nanocrystals in Fe_3O_4@PPy/Pd nanocomposites synthesized in mixed solvent with the ethanol/water volume ratio at 1:1.

Effect of the Solvent Ratio on the Structure of Fe_3O_4@PPy/Pd nanocomposites

The solvent utilized for pyrrole polymerization has commonly a considerable impact on the microstructure and surface morphology of the resultant polymer by finely tuning the nucleation and growth rates of polymer.[51, 52] Fig. 2 displays the TEM images of Fe_3O_4@PPy/Pd nanocomposites at different ethanol/water volume ratios.

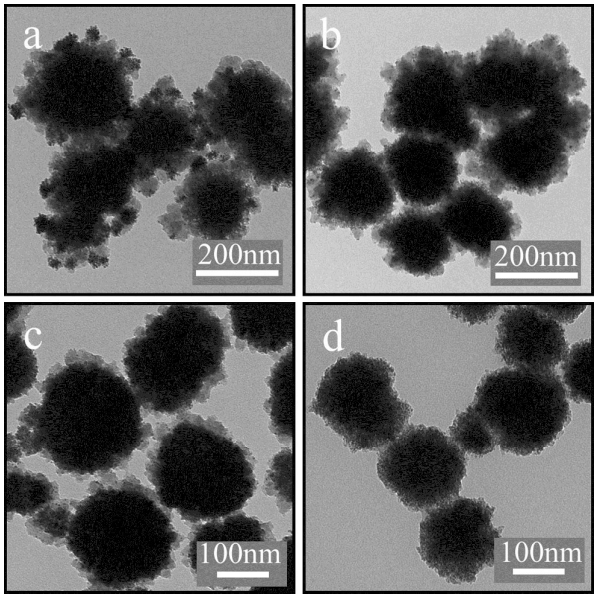

Fig. 2 TEM images of Fe_3O_4@PPy/Pd nanocomposites fabricated in mixed solvents with the ethanol/water volume ratio at 0:1 (a), 1:1 (b), 2:1 (c), 1:0 (d).

As show in Fig. 2, with the increase in the ethanol/water ratio, the number and size of PPy satellites onto Fe_3O_4 nanoclusters decreases gradually and the morphology of Pd nanoparticles changes from large aggregates to single nanoparticle. When using pure ethanol as the reaction medium, no any PPy or Pd nanoparticle onto Fe_3O_4 nanoclusters was observed. Clearly, the structure of Fe_3O_4@PPy/Pd nanocomposites is dependent directly on the ethanol/water ratio, which could be explained by two main effects. On the one hand, the solubility parameter of pyrrole (21.5 $MPa^{1/2}$)[53] is relatively near to that of absolute ethanol (26.1 $MPa^{1/2}$)[54] and greatly different to that of pure water (47.8 $MPa^{1/2}$)[54], according to the solubility parameters in Table 1, indicating that there is a stronger tendency to form solely in the reaction medium than to deposit onto Fe_3O_4 nanoclusters for PPy in terms of the consistency principle with increasing the alcoholic amount in the reaction medium. On the other hand, the generation of pyrrole dimer combined by the cation radicals of pyrrole is commonly the rate controlling step for the final PPy.[55] The higher dielectric constant of water (78 at 25 °C)[56] than that of ethanol (24.5 at 25 °C)[56] means that water rather than ethanol could reduce the coulomb repulsion between cation radicals to promote their combination, thus enhancing the polymerization of pyrrole monomer. As shown in Fig. 2a, too high polymerization rate of pyrrole monomer in pure water results in the too high generation rate of Pd nanocrystals reduced by H_2PdCl_4, thereby leading to the formation of numerous aggregates of Pd nanocrystals in PPy matrixes. With increasing the alcoholic amount in mixed solvents, the redox rate between pyrrole monomer and H_2PdCl_4 goes down to reach an approximate value, thereby resulting in the generation of multiple uniform Pd nanocrystals homogeneously into PPy satellites onto Fe_3O_4 nanoclusters in Fig. 2b and c. However, no any PPy or Pd nanocrystals is formed onto Fe_3O_4 nanoclusters in absolute ethanol in Fig. 2d, which means the polymerization of pyrrole oxidized by H_2PdCl_4 is strongly suppressed by absolute ethanol.

Table 1 Solubility Parameters (δ) of pyrrole monomer and mixed solvents

	Pyrrole	*Ethanol/ H_2O (0:1)*	*Ethanol/ H_2O (1:1)*	*Ethanol/ H_2O (2:1)*	*Ethanol/ H_2O (1:0)*
Solubility parameter [(cal/cm^3)$^{1/2}$](δ1)	10.5[a]	--	--	--	--
Solubility parameter [(MPa)$^{1/2}$](δ2)	21.5	47.8	37.0	33.3	26.1

[a] The values were determined in accordance to this equation: $(δ1)^2*4.19=(δ2)^2$.

Effect of the molar ratio of pyrrole/H_2PdCl_4 on the structure of Fe_3O_4@PPy/Pd nanocomposites

In general, the amount of noble-metal precursor plays an crucial role in the metal loading for metal-based heterogeneous catalyst.[20] Fig. 3 reveals the TEM images of Fe_3O_4@PPy/Pd nanocomposites prepared at different molar ratios of pyrrole to H_2PdCl_4 when using

ethanol/water of the volume ratio at 1/1 as the reaction medium and unchanging other reaction conditions. It is clearly found that all the samples synthesized at different molar ratio of pyrrole/H_2PdCl_4 show a typical core-satellite structure, in which single Fe_3O_4 nanocluster is an inner core and multiple PPy/Pd nanocoposites are satellites. Multiple uniform Pd nanocrystals are homogeneously confined into single PPy particle in every satellite. To identify the Pd loading of magnetic nanocompsites formed at different pyrrole/H_2PdCl_4 ratios, inductively coupled plasma (ICP) analysis was performed. By simply tailoring the molar ratio of pyrrole/H_2PdCl_4 from 10:1, 7.5:1 to 5:1 and unchanging the amount of pyrrole, the Pd loading of magnetic nanocomposites goes up gradually from 3.08, 3.94, and 4.70 wt%, consistent with an increase in the amount of Pd precursor, H_2PdCl_4. However, the Pd loading of magnetic nanocomposites instead declines to 2.82 wt% when the amount of H_2PdCl_4 continues to increase until the molar ratio of pyrrole/H_2PdCl_4 reaches 2.5:1. Because the excessive feeding amount of H_2PdCl_4 accelerates simultaneously the polymerization of pyrrole and the generation of Pd nanocrystals, resulting in the generation of many soluble PPy molecules with short chains in the reaction medium. These soluble PPy molecules together with partial Pd nanocrystals confined into them could not be deposited onto Fe_3O_4 nanoclusters in the whole redox process, therefore resulting in a sharp decline in the Pd content of the resultant Fe_3O_4@PPy/Pd nanocomposites.

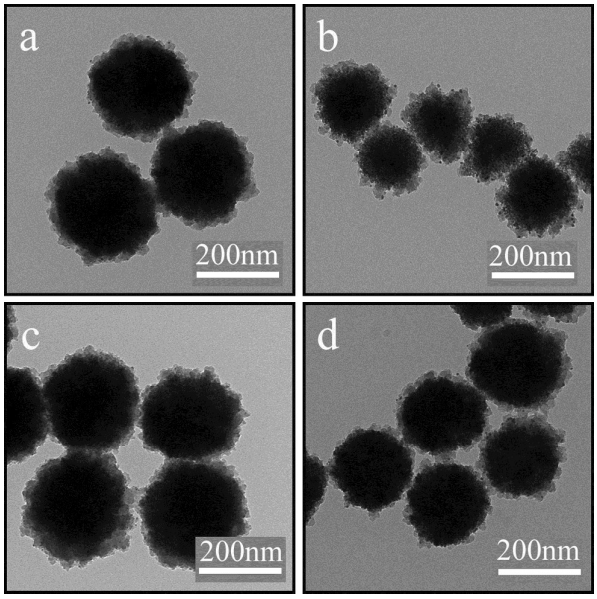

Fig. 3 TEM images of Fe_3O_4@PPy/Pd nanocomposites at different molar ratio of pyrrole to H_2PdCl_4: 10:1 (a), 7.5:1 (b), 5:1 (c), 2.5:1 (d).

Catalytic activities of Fe_3O_4@PPy/Pd nanocomposites

The catalytic hydrogenation of nitroaromatic compounds is commonly used as the model reactions to evaluate the activity of noble-metal nanoparticles.[57] In this study, the reduction of 2-Nitroaniline (2-NA) to 1, 2-benzenediamine with excess of $NaBH_4$ at room temperature was utilized to investigate the catalytic activity of the Fe_3O_4@PPy/Pd nanocomposites with the Pd loading of 4.70 wt%, as monitored by UV/Vis spectroscopy (Fig. 4). As revealed in Fig. 4a, there is no any obvious change in the color of the mixture of 4-NP and $NaBH_4$ for a couple of days without the catalyst, indicating the reaction did not occur. After a small amount of the suspension of Fe_3O_4@PPy/Pd (0.1 mL, $4.42*10^{-6}$ mmol of Pd, 0.0442 mol%) was added, the color of the above mixture altered from yellow to colorless with the prolonged reaction time, which corresponds to a gradual decline in a typical peak of 2-NA at 414.5 nm, indicating the complete reduction of 2-NA to 1, 2-benzenediamine. Considering the far higher concentration of $NaBH_4$ than that of 2-NA (CNaBH4/C2-NA=400), the reduction of 2-NA was regarded as a pseudo-first-order reaction. Fig. 4c just reveals a linear relation between ln (C_t/C_0) and the reaction time (t), where C_0 and C_t correspond to the absorbance of 2-NA at 0 and t min, respectively. The kinetic reaction rate constant *k* was determined to be 0.23 min^{-1} according to the rate equation of the pseudo-first-order reaction, ln (C_t/C_0) = $-k \cdot t$. The turnover frequency (TOF) of the Pd-based catalyst for the 2-NA reduction was determined to be up to 12168 h^{-1}, which confirms that Fe_3O_4@PPy/Pd nanocomposite is highly efficient for the reduction of 2-NA.

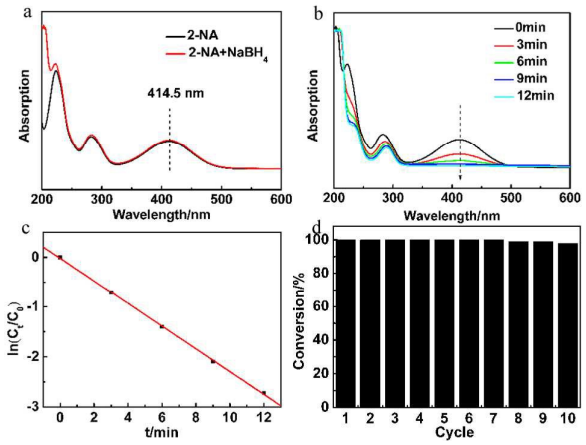

Fig. 4 UV/Vis spectra of 2-NA and the mixture of 2-NA and $NaBH_4$ (a), Time-dependent UV/Vis spectra of 4-NP catalyzed by Fe_3O_4@PPy/Pd nanocomposite (b), The plot of ln(C_t/C_0) against the reaction time (t) for the reduction of 2-NA (c), Conversion of 2-NA in the presence of Fe_3O_4@PPy/Pd nanocomposite (d).

Stability is commonly one of major issues concerning highly efficient catalysts. Thus, the reduction of 2-NA by $NaBH_4$ was also utilized to evaluate the durability of the Pd-based catalyst. As shown in Fig. 4d, the conversion of the nanocatalyst still retains almost 100 % after over ten successive catalytic cycles, indicating its superior stability due to the confinement of tiny Pd nanocystals uniformly into small PPy satellites against the migration, agglomeration and even loss of catalytically active sites. The SEM images (Fig. S11a, b) show that the recovered catalyst still preserves their initial core-satellites structure and the EDS mapping image(Fig. S11c) reveals that Pd species are still uniformly distributed into the recovered catalyst after ten cycles. Meanwhile, XRD pattern of the recovered catalyst (Fig. S12) is similar to that of the fresh catalyst, indicating no occurrence of large Pd aggregates. However, the TEM image (Fig. S11d) shows that a small fraction of Pd particles becoming larger. It is possibly because the collision between the substrate molecules and the active Pd surfaces weakens the Pd-

pyrrole interaction during catalytic reaction,[17] thereby leading to partial migration of some Pd nanocrystals dispersed on the surface of PPy and subsequent formation of small aggregates. The results mentioned above verifies relatively high stability of the catalyst with only light aggregation due to the confinement of the majority of tiny Pd nanocystals uniformly into small PPy satellites against the migration, agglomeration and even loss of catalytically active sites. The XPS spectra of Pd 3d core electrons in the recovered catalyst (Fig. S13) could be deconvoluted into four peaks. The peaks at 335.7 (Pd 3d 5/2) and 340.9 eV (Pd 3d 3/2) are attributed to metallic Pd (0),[58] and the peaks at 337.8 (Pd 3d 5/2) and 343.1 eV (Pd 3d 3/2) are attributed to Pd (II) species, indicating the existence of PdO due to partial oxidation of small Pd nanocystals with abundant active surface sites.[35] When the Pd-based nanocatalyst was used for the continual catalytic cycles, magnetic separation provides a rapid recoverability for catalyst (Fig. 5 inset) due to its strong magnetic response, consistent with the specific saturation magnetization of up to 41 emu/g determined by VSD in Fig. 5. The magnetization hysteresis loop of the Pd-based nanocatalyst also exhibits its perfect superparamagnetism, which could ensure fine redispersion of recovered magnetic nanocatalysts into the reaction medium on removal of the external magnet,[1] thereby delivering efficiently the activity of Pd nanocrystals in recycling catalysis.

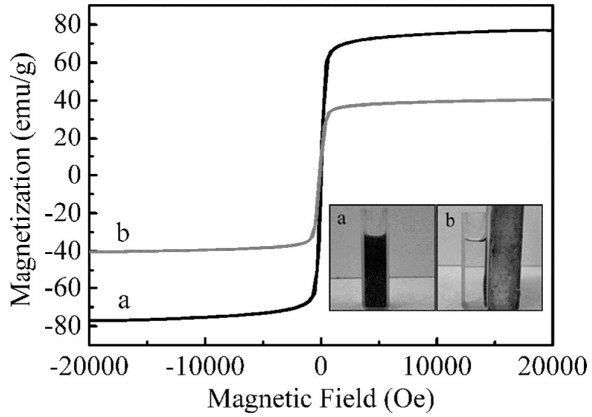

Fig. 5 Magnetic hysteresis loops of PAA-modified Fe_3O_4 nanoclusters (a) and Fe_3O_4@PPy/Pd nanocomposite (b) at 300 K. The insets reveal separation photos of Fe_3O_4@PPy/Pd nanocatalyst; inset (a) and inset (b) correspond to the photo before using a magnet and about 15 s after using a magnet, respectively.

To further investigate its activity, the magnetic nanocatalyst was also extended to catalytic reductions of many other nitroaromatic compounds, such as 4-Nitrophenol (4-NP), 3-Nitropheol (3-NP), 2-Nitrophenol (2-NP), 4-Nitroaniline (4-NA), 3-Nitroamine (3-NA), 1-Chloro-2-nitrobenzene, and 2-Amino-5-nitrophenol, as shown in Fig. S4-S10. The kinetic constant (*k*) and TOF values of each reaction were listed in Table 2, and the TOF of each reaction is up to 6902 h^{-1}, 11280 h^{-1}, 6370 h^{-1}, and 16979 h^{-1}, 3134 h^{-1}, 24420 h^{-1}, 14760 h^{-1}, respectively. In comparison with the recently reported Pd-supported catalysts for the reduction of 4-NP, such as RGO@Pd@C (273.6 h^{-1} of TOF),[59] Pd/SnO2/polyaniline (493.2 h^{-1} of TOF),[60] Pd-ZnO (518.4 h^{-1} of TOF),[61] Pd /CNT-220 (1080 h^{-1} of TOF),[62] Pd/Fe_3O_4/graphene (5296 h^{-1} of TOF),[63] Pd/SnO_2/graphene (6120 h^{-1} of TOF),[64] Pd/Click-Polymer(7 500 and 22500 h^{-1} of TOF),[65] the as-synthesized Fe_3O_4@PPy/Pd nanocomposite exhibits relatively high activity (6902 h^{-1} of TOF). The outstanding catalytic activity could be probably attributing to the magnetic nanocomposite with unique core-satellites structure, since the substrates around the magnetic nanocomposite could take the relatively short transport length towards tiny Pd nanocrystals embedded into small PPy particles.

Table 2 Kinetic reaction rate constants and TOFs of the reduction of nitroaromatic compounds, such as 2-NP, 3-NP, 4-NP, 3NA, 4-NA, 1-Chloro-2-nitrobenzene, and 2-Amino-5-nitrophenol by $NaBH_4$ in the presence of Fe_3O_4@PPy/Pd nanocomposite

Substitutes	k/min^{-1}	TOF/h^{-1}
2-NP	0.12	6370
3-NP	0.21	11280
4-NP	0.13	6902
3-NA	0.058	3134
4-NA	0.32	16979
1-Chloro-2-nitrobenzene	0.47	24420
2-Amino-5-nitrophenol	0.28	14760

Conclusion

In summary, we have developed a facile soft template-assisted strategy combined with a redox reaction to fabricate Fe_3O_4@PPy/Pd nanocomposites with single Fe_3O_4 nanocluster as inner core and multiple PPy/Pd particles as satellites, in which multiple tiny Pd nanocrystals are uniformly confined into single small PPy particle. The water/ethanol ratio significantly influences the redox reaction rate between pyrrole monomer and Pd precursor, and ultimately tunes the morphology of magnetic nanocomposites and the dispersity of Pd nanocrystals in PPy matrix. Meanwhile, the Pd loading of magnetic nanocomposites could be finely tailored by simply altering the molar ratio of pyrrole/H_2PdCl_4. Finally, the Pd-based nanocatalyst displays superior activity, magnetic recoverability, and robust stability, with respect to the reduction of many nitroaromatic compounds such as 2-NA, 3-NA, 4-NA, 2-NP, 3NP, 4-NP, 1-Chloro-2-nitrobenzene, and 2-Amino-5-nitrophenol, owing to the unique core-satellites structure of magnetic nanocomposite. Superior activity stems from the short diffusion route of substitutes around PPy satellites toward Pd nanocrystals confined into each small PPy satellite, and high stability results from the confinement of Pd nanocrystals into PPy matrix against migration, aggregation and even loss during the catalytic conversions. Ongoing research is synthesis and application of Fe_3O_4@PPy/M (M=Au or Pt) nanocomposites with single Fe_3O_4 inner core and multiple PPy/M satellites, in each of which multiple ultrafine M nanoparticles in an individual form are spatially confined into single PPy particle.

Acknowledgements

This study was granted by National Natural Science Foundation of China (Grant No. 51503178), Natural Science Foundation of Hebei Province (No. E2015203114), China Postdoctoral Science Foundation (No. 2015M571278), Postdoctoral Science Foundation of Hebei Province (B2014003009), Science and Technology Research and Development Program of Qinhuangdao (201401A049), Independent Research Project of Yanshan University for Young Teachers (14LGB019) and the Doctor Foundation of Yanshan University (B789).

References

1. C. Lim and I. Lee, *Nano Today,* 2010, **5**, 412-434.
2. V. Polshettiwar, R. Luque, A. Fihri, H. Zhu, M. Bouhrara, J. Basset, *Chem. Rev.,* 2011, **111**, 3036-3075.
3. M. Gawande, P. Branco and R. Varma, *Chem. Soc. Rev.*, 2013, **42**, 3371-3393.
4. D. Wang and D. Astruc, *Chem. Rev.,* 2014, **114**, 6949-6985.
5. L. Rossi, N. Costa, F. Silva and R. Wojcieszak, *Green Chem.*, 2014, **16**, 2906-2933.
6. S. Tsang, V. Caps, I. Paraskevas, D. Chadwick and D. Thompsett, *Angew. Chem. Int. Ed.*, 2004, **43**, 5645-5649.
7. Q. Kainz, R. Linhardt, R. Grass, G. Vilé, J. Pérez-Ramírez, W. Stark and O. Reiser, *Adv. Funct. Mater.,* 2014, **24**, 2020-2027.
8. H. Yoon, S. Ko and J. Jang, *Chem. Commun.,* 2007, 1468-1470.
9. Q. An, M. Yu, Y. Zhang, W. Ma, J. Guo and C. Wang, *J. Phys. Chem. C*, 2012, **116**, 22432-22440.
10. D. Yi, S. Lee and J. Ying, *Chem. Mater.,* 2006, **18**, 2459-2461.
11. Z. Zhang, Y. Zhou, Y. Zhang, S. Zhou, S. Xiang, X. Sheng and P. Jiang, *J. Mater. Chem. A*, 2015, **3**, 4642-4651.
12. N. Costa, P. Kiyohara, A. Monteiro, Y. Coppel, K. Philippot and L. Rossi, *J. Catal.,* 2010, **276**, 382-389.
13. M. Guerrero, N. Costa, L. Vono, L. Rossi, E. Gusevskayad and K. Philippot, J. *Mater. Chem. A,* 2013, **1**, 1441-1449.
14. H. Zhang, X. Zhong, J. Xu and H. Chen, *Langmuir,* 2008, **24**, 13748-13752.
15. S. Xuan, Y. Wang, J. Yu and K. Leung, *Langmuir*, 2009, **25**,11835-11843.
16. B. Liu, W. Zhang, F. Yang, H. Feng and X. Yang, *J. Phys. Chem. C*, 2011, **115**, 15875-15884.
17. J. Ge, Q. Zhang, T. Zhang and Y. Yin, *Angew. Chem. Int. Ed.,* 2008, **47**, 8924-8928.
18. Y. Deng, Y. Cai, Z. Sun, J. Liu, C. Liu, J. Wei, W. Li, C. Liu, Y. Wang and D. Zhao, *J. Am. Chem. Soc.*, 2010, **132**, 8466-8473.
19. Z. Sun, J. Yang, J. Wang, W. Li, S. Kaliaguine, X. Hou, Y. Deng and D. Zhao, *J. Mater. Chem. A*, 2014, **2**, 6071-6074.
20. T. Yao, T. Cui, X. Fang, F. Cui and J. Wu, *Nanoscale*, 2013, **5**, 5896-5904.
21. W. Hu, B. Liu, Q. Wang, Y. Liu, Y. Liu, P. Jing, S. Yu, L. Liu and J. Zhang, *Chem.Commun.*, 2013, **49**, 7596-7598.
22. K. Lee, B. Lee, K. Lee, M. Yi and N. Hur, *Chem. Commun.,* 2012, **48**, 4414-4416.
23. H. Zhang, S. Qi, X. Niu, J. Hu, C. Ren, H. Chen and X. Chen, *Catal. Sci. Technol.*, 2014, **4**, 3013-3024.
24. F. Ke, L. Wang and J. Zhu, *Nanoscale*, 2015, **7**, 1201-1208.
25. T. Yao, T. Cui, H. Wang, L. Xu, F. Cui and J. Wu, *Nanoscale,* 2014, **6**, 7666-7674.
26. X. Zhang, M. Lin, X. Lin, C. Zhang, H. Wei, H. Zhang and B. Yang, *ACS Appl. Mater. Interfaces,* 2014, **6**, 450−458.
27. W. Guo, Q. Wang, G. Wang, M. Yang, W. Dong and J. Yu, *Chem. Asian J.,* 2013, **8**, 1160-1167.
28. W. Guo, Q. Wang, Y. Luan, G. Wang, W. Dong and J. Yu, *Chem. Asian J.,* 2015, **10**, 701-708.
29. Y. Xue, X. Lu, X. Bian, J. Lei and C. Wang, *J. Colloid Interface Sci.,* 2012, **379**, 89-93.
30. M. Góral-Kurbiel, A. Drelinkiewicz, R. Kosydar, B. Dembińska, P. Kulesza and J. Gurgul, *Electrocatalysis,* 2014, **5**, 23-40.
31. A. Salabat, F. Mirhoseini, M. Mahdieh and H. Saydi, New J. Chem., 2015, **39**, 4109-4114.
32. X. Lu, X. Bian, G. Nie, C. Zhang and C. Wang, *J. Mater. Chem.,* 2012, **22**, 12723-12730.
33. S. Yang, C. Shen, Y. Liang, H. Tong, W. He and X. Shi, *Nanoscale,* 2011, **3**, 3277-3284.
34. S. Vasilyeva, M. Vorotyntsev, I. Bezverkhyy, E. Lesniewska, O. Heintz and R. Chassagnon, *J. Phys. Chem. C,* 2008, **112**, 19878-19885.
35. V. Zinovyeva, M. Vorotyntsev, I. Bezverkhyy, D. Chaumont and J. Hierso, *Adv. Funct. Mater.,* 2011, **21**, 1064-1075.
36. S. Fujii, S. Matsuzawa, Y. Nakamura, A. Ohtaka, T. Teratani, K. Akamatsu, T. Tsuruoka and H. Nawafune, *Langmuir*, 2010, **26**, 6230-6239.
37. S. Fujii, S. Matsuzawa, H. Hamasaki, Y. Nakamura, A. Bouleghlimat and N. Buurma, *Langmuir*, 2012, **28**, 2436-2447.
38. S. Fujii, H. Hamasaki, H. Abe, S. Yamanaka, A. Ohtaka, E. Nakamura and Y. Nakamura, *J. Mater. Chem. A,* 2013, **1**, 4427-4430.
39. T. Yao, H. Wang, Q. Zuo, J. Wu, X. Zhang, F. Cui and T Cui, *Chem. Asian J.,* 2015, **10**, 1940-1947.
40. F. Gaeta, G. Perna and G. Scala, *J. Polym. Sci. Part B: Polym. Phys.*, 1975, **13**, 203-222.
41. J. Séquaris, F. Baßmann, A. Hild, H. Narres and M. Schwuger, *Colloids Surf. A*, 1999, **159**, 503-512.
42. X. Zhang, H. Chen and H. Zhang, *Chem. Commun.*, 2007, 1395-1405.
43. G. Dudek and R. Holm, *J. Am. Chem. Soc.*, 1961, **83**, 2099-2104.
44. X. Zhang, H. Tong, S. Liu, G. Yong and Y. Guan, *J. Mater. Chem. A*, 2013, **1**, 7488-7493.
45. H. Liu, L. Zhang, N. Wang and D. Su, *Angew. Chem. Int. Ed.,* 2014, **53**, 12634-12638.
46. S. Guo, S. Dong and E. Wang, *Chem. Eur. J.,* 2009, **15**, 2416-2424.
47. E. Brancewicz, E. Gradzka, A. Wilczewska and K. Winkler, *ChemElectroChem*, 2015, **2**, 253-262.
48. J. Stejskal, M.Trchovà, I. Ananieva, J. Janča, J. Prokeš, S. Fedorova and I. Sapurina, *Synth. Met.*, 2004, **146**, 29-36.
49. X. Yang and L. Li, *Synth. Met.*, 2010, **160**, 1365-1367.
50. C. Saravanan, R. Shekhar and S. Palaniappan, *Macromol. Chem. Phys.*, 2006, **207**, 342-348.
51. S. Sadki, P. Schottland, N. Brodie and G. Sabouraud, *Chem. Soc. Rev.*, 2000, **29**, 283-293.

52. A. Pich, Y. Lu, H. Adler, T. Schmidt and K. Arndt, *Polymer*, 2002, **43**, 5723-5729.
53. S. Im and S. B yun, *J. Appl. Polym. Sci.*, 1994, **51**, 1221-1229.
54. C. Hansen in Hansen Solubility Parameters: A User's Handbook, CRC, New York, 2007, 55-56.
55. T. Vernitskaya and O. Efimov, *Russ. Chem. Rev.*, 1997, **66**, 443-457.
56. A. Ben-Naim, *J. Chem. Phys.*, 1977, **67**, 4884-4890.
57. H. Hu, J. Xin, H. Hu, X. Wang, D. Miao and Y. Liu, *J. Mater. Chem. A*, 2015, **3**, 11157-11182.
58. I. Aruna, B. R. Mehta, L. Malhotra and S. Shivaprasad, *J. Appl. Phys.,* 2008, **104**, 064308.
59. Z. Zhang, F. Xiao, J. Xi, T. Sun, S. Xiao, H. Wang, S. Wang and Y. Liu, *Sci. Rep.,* 2014, **1**, 4053-4058.
60. X. Lu, Y. Xue, G. Nie and C. Wang, *Catal. Lett.,* 2012, **142**, 566-572.
61. Y. Jin, J. Xi, Z. Zhang, J. Xiao, F. Xiao, L. Qian and S. Wang, *Nanoscale,* 2015, **7**, 5510-5515.
62. X. Gu, W. Qi, X. Xu, Z. Sun, L. Zhang, W. Liu, X. Pan and D. Su, *Nanoscale,* 2014, **6**, 6609-6616.
63. X. Li, X. Wang, S. Song, D. Liu and H. Zhang, *Chem.-Eur. J.,* 2012, **18**, 7601-7607.
64. H. Li, S. Gan, D. Han, W. Ma, B. Cai, W. Zhang, Q. Zhang and L. Niu, *J. Mater. Chem. A,* 2014, **2**, 3461-3467.
65. C. Deraedt, L. Salmon, J. Ruiz and D. Astruc, *Adv. Synth. Catal.,* 2013, **355**, 2992-3001.

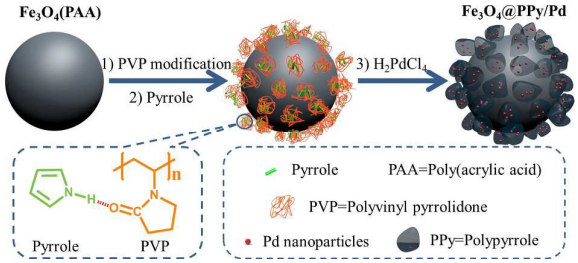

A soft template-assisted redox strategy has been developed to fabricate core-satellites Fe_3O_4@PPy/Pd nanocomposites as efficient nanocatalysts for reduction of nitroaromatics.